Initial Growth of N,NBis(1-ethylpropyl)perylene-3,4,9,10-tetracarboxdiimide Films on Cu(100)

4 AUTHORS, INCLUDING:

O. Grizzi
Centro Atómico Bariloche
105 PUBLICATIONS **959** CITATIONS

SEE PROFILE

maria luz Martiarena
National Scientific and Technical Research Co…
50 PUBLICATIONS **323** CITATIONS

SEE PROFILE

E.A. Sánchez
Centro Atómico Bariloche
94 PUBLICATIONS **586** CITATIONS

SEE PROFILE

Initial Growth of *N,N′*-Bis(1-ethylpropyl)perylene-3,4,9,10-tetracarboxdiimide Films on Cu(100)

J. C. Moreno-López, O. Grizzi, M. L. Martiarena, and E. A. Sánchez*

Centro Atómico Bariloche - Instituto Balseiro - CNEA - UNCuyo - CONICET, Avda. Ezequiel Bustillo 9500, 8400 S.C. de Bariloche, Río Negro, Argentina

ABSTRACT: We have studied the initial stages of the adsorption of *N,N′*-bis(1-ethylpropyl)-perylene-3,4,9,10-tetracarboxdiimide (EP-PTCDI) on Cu(100) using scanning tunnelling microscopy (STM), X-ray photoelectron spectroscopy (XPS), low-energy electron diffraction (LEED), and density functional theory (DFT) calculations. STM images show that the EP-PTCDI molecules initially absorb on the surface, forming ordered islands, without preferential nucleation at the step-edges of the terraces as is the case for adsorption of the same molecule on Ag(111). The 2D islands grow upon the completion of the surface with a single-molecular layer. The experimental and simulated LEED patterns show that the molecular arrangement within the islands can be explained by a commensurate superstructure and its four rotational equivalents. The electron spectroscopies show net charge transfer from the surface to the molecule and a decrease of about 0.7 eV in the work function (from 4.59 to 3.9 eV) after a single-layer adsorption. The DFT calculations for the adsorption of a single layer qualitatively reproduce the features observed in STM images and allow us to explain the observed charge exchange behavior together with the work function change.
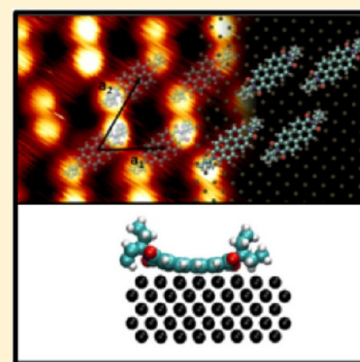
1. INTRODUCTION

Organic molecules like perylenetetracarboxylic diimides (PTCDIs) have been used in applications in organic field effect transistors (OFETs),[1−3] solar cells,[4,5] and organic light-emitting diodes (OLEDs),[6−9] among others. These molecules are very good and versatile candidates for organic optoelectronic applications due to their electronic, optical, and charge transport properties[10] and to their commercial availability and low cost. To improve the functionality of the devices, the PTCDI molecules are usually tailored either by the introduction of appropriate substituents in the imide position or by the core substitution in the bay region. Very recently, it was demonstrated that *N,N′*-bis(1-ethylpropyl)-perylene-3,4,9,10-tetracarboxdiimide (EP-PTCDI) films have efficient performance for optoelectronic devices,[11,12] but the detailed characteristics of the layer formation and the interaction with different noble metals are still unknown. In particular, it is interesting to study how the ethylpropyl (EP-) end groups might affect order, taking into account that the mobility of the molecules on the surface and the lateral intermolecular interaction can be reduced by the presence of the end groups, as it was observed for dimethyl-PTCDI (DiMe-PTCDI) molecules.[13,14]

In this work we report the experimental and theoretical study of the initial growth stages of EP-PTCDI on a Cu(100) surface by using complementary techniques: scanning tunnelling microscopy (STM), low energy electron diffraction (LEED), X-ray photoelectron spectroscopy (XPS), and density functional theory (DFT) calculations that include van der Waals interactions. STM and LEED experiments provided information about the adsorption kinetics and the ordering, while the electron spectroscopies gave information about the charge transfer between the surface and the molecule and the surface work function changes after molecule adsorption. DFT calculations provided information on the geometrical configuration adopted by the EP-PTCDI molecule on the Cu(100) surface, as well as details on the electron density and the ionic charge that help to interpret the different features observed in the dual scan mode STM images and in electron spectroscopies.

## 2. EXPERIMENTAL AND THEORETICAL METHODS

2.1. Experiment. STM and LEED measurements were carried out in an ultrahigh vacuum (UHV) chamber (base pressure ~10^{-10} mbar) equipped with a variable-temperature scanning tunnelling microscope (VT-STM) and a low energy electron diffraction (LEED) system (both from Omicron Nanotechnology). The STM images were acquired in a constant current mode using electrochemical etched tungsten tips, with the sample held at room temperature. The images were processed using the WS×M free software.[15]

XPS measurements were performed in a second UHV chamber equipped with an Al Kα X-ray anode (1486.5 eV) and a CLAM100 VG Scientific hemispherical energy analyzer, with the sample grounded. The work function changes were measured from the shift of the onset of the secondary electron energy distribution (very low energy region of the electron
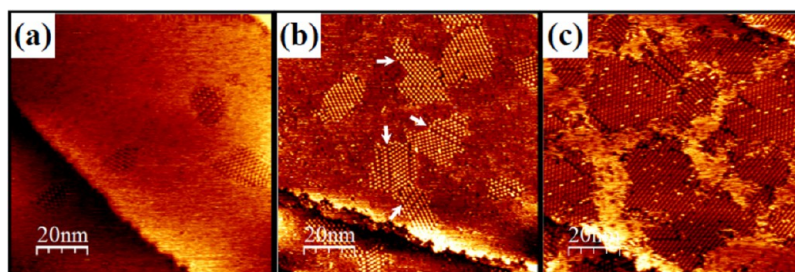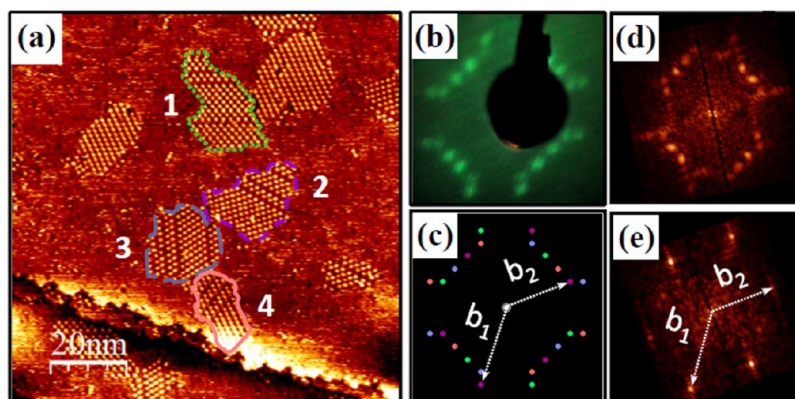
Figure 1. STM images of EP-PTCDI deposited on Cu(100) at 300 K: (a) 0.06 ML, (b) 0.2 ML, and (c) ~0.7 ML. Some dislocations within the islands are marked by white arrows in panel (b). The images were acquired at I_T = 60 pA and V_S = +0.3, +0.5, and +0.2 V, respectively.

Figure 2. (a) STM image after the deposition of 0.2 ML of EP-PTCDI on Cu(100). The image was acquired at V_S = +0.5 V and I_T = 60 pA. (b) Experimental LEED pattern recorded at 13.6 eV at nearly normal incident. (c) Simulated LEED pattern of the superstructure $\begin{pmatrix} 3 & 4 \\ -2 & 6 \end{pmatrix}$. Spots of the same color in (c) indicate equivalent domains. (d) and (e): 2D-FFT spectrum performed over all the islands and in island labeled 2 of panel (a), respectively.

spectra) produced by the X-ray bombardment. In this case, the sample was polarized with −5 V with respect to the grounded entrance slit of the electron analyzer, to ensure that electrons emitted from the sample have energies high enough to overcome the work function of the analyzer.

The Cu(100) single crystal was obtained from Mateck GmbH.[16] Its surface was cleaned by cycles of 1.5 keV Ar⁺ ion bombardment followed by annealing at 800 K. The temperature was measured by means of a chromel−alumel thermocouple attached to the sample holder. The organic EP-PTCDI molecule (also named as 2,9-di(pent-3-yl)anthra-(2,1,9-def:6,5,10-d′e′f′)diisoquinoline-1,3,8,10-tetrone, Catalogue No. ST 1/23) was synthesized and provided by Sensient Imaging Technologies GmbH[17] as a red powder. The EP-PTCDI molecules were deposited onto the clean surface using a Knudsen-cell evaporator equipped with a ceramic crucible, at a deposition rate of ~5.0×10^{-3} ML/s. Before evaporation the EP-PTCDI powder was degassed for about 1 h to remove contaminants, allowing us to keep the pressure in the low 10^{-9} mbar range during evaporations. The reported coverages were determined from a direct analysis of the STM images, defining an EP-PTCDI monolayer (ML) as the amount of deposited material that just covers the whole surface with a single molecular layer. Since for coverages larger than 1 ML the thin film grows forming 3D islands,[18,19] we expressed the coverage in terms of equivalent monolayer, i.e., in terms of the amount required to get that coverage if the growth was layer-by-layer.

2.2. Theory. The DFT calculations have been carried out within the slab-supercell approach by using the Vienna ab initio simulation program (VASP).[20,21] The one-electron Kohn−

Sham orbitals are expanded in a plane-wave basis set, and electron−ion interactions are described through the PAW_PBE pseudopotentials.[22,23]

Exchange and correlation (XC) is described within the van der Waals density functional (vdW-DF)[24] with optB86b as the exchange functional.[25] The sampling of the Brillouin zone is carried out according to the Monkhorst−Pack method.[26] The chosen cutoff energy is 450 eV; electron smearing is introduced following the Methfessel−Paxton technique[27] with $\sigma = 0.2$ eV; and all the energies are extrapolated to 0 K. The convergence of the energy is kept always on the order of 10^{-4} eV, and the minimization of the forces is assured up to the order of 10^{-1} eV/nm.

We use the Bader method to calculate the charge around the atoms.[28] The Bader analysis has been done considering the total charge density (core plus valence charge density). The STM images were simulated within the Tersoff−Hamann approach[29] where the partial charge density is proportional to the tunneling current at the position of the STM tip.

For bulk Cu, by using a cutoff energy of 750 eV and a 16 × 16 × 16 k-point mesh we obtained a lattice parameter a_{Cu} of 0.360 nm. This result is in excellent agreement with the experimental value of 0.3615 nm at room temperature.[30] The results for the EP-PTCDI adsorption on Cu(100) are presented in the next section.

3. RESULTS AND DISCUSSION

Figure 1 shows STM images corresponding to the initial growth stages of EP-PTCDI on Cu(100) as a function of the surface coverage. Figures 1a and 1b show that the EP-PTCDI

molecules initially adsorb somewhere in the middle of the terraces, forming ordered islands. No preferential nucleation at the step-edges of the terraces, like in the case of Ag(111),[18] was observed. As the deposition continues, new islands nucleate on the terraces which grow laterally covering the substrate with a single monolayer (2D growth). The aggregation in two-dimensional islands indicates that molecules that arrive on top of an existing island have enough mobility to reach the island-edges and to hop off the island, in agreement with a relatively small Ehrlich−Schwoebel barrier.[31] A similar trend has also been observed for the case of EP-PTCDI on Ag(111) where a constant sticking probability has been measured until the completion of the first monolayer.[19] The apparent height (the mean height given by the STM at a constant current measurement mode) of the EP-PTCDI islands is about 0.17 ± 0.03 nm, consistent with an adsorption geometry in which the perylene core plane is almost parallel to the surface.[18]

The islands show one ordered structure but oriented in four directions. This order is occasionally perturbed by dislocation lines running along one of the main directions of the islands (see white arrows in Figure 1b). In Figure 2a, we present an STM image with these four domains formed in a single atomic terrace, labeled from 1 to 4. We found that the island labeled 1 is rotated about 37° with respect to the island 2, and those islands are rotated 90° with respect to islands 3 and 4, respectively. To get information about the molecular structure within the islands, and their arrangements with respect to the substrate, we performed LEED measurements. The clear and separated spots in the LEED pattern shown in Figure 2b are indicative of a high-quality arrangement of the monolayer for extended areas on the surface. The interpretation of this experimental LEED pattern is not straightforward, so we have performed many simulations with the LEEDPat3 software.[32] The best agreement between the simulated pattern and the experimental one is shown in Figure 2c, indicating that the arrangement of the EP-PTCDI molecule on Cu(100) can be explained by a commensurate superstructure $\begin{pmatrix} 3 & 4 \\ -2 & 6 \end{pmatrix}$ and its four rotational equivalents. This matrix corresponds to an arrangement in the real space represented by a unit cell with lattice constants, $\mathbf{a}_1$ = 1.27 nm, $\mathbf{a}_2$ = 1.61 nm, and γ = 55.3°, that are in very good agreement with our STM measurements. In addition, the rotation of the four domains, two rotated at 36,46° between them, and the other two rotated 90° with respect to those ones, also fit very well with our experimental observations. Finally, to compare the symmetry of the structure observed in the STM images with those of the LEED patterns, the 2D fast fourier transform (2D-FFT) of the four different islands, and islands labeled 2 (violet spots), are, respectively, shown in Figures 2d and 2e.

To obtain the single-molecule geometrical configuration, we calculated by DFT a full relaxation of all atom coordinates in a unit cell of 3.10×2.20 nm^2 and a vacuum layer with a thickness of 2.90 nm using a $1 \times 1 \times 1$ k-point mesh.[33] Then, the monolayer of EP-PTCDI molecules adsorbed onto a Cu(100) surface was taken into account by considering a slab of five layers of Cu(100) in a molecule unit cell using a $5 \times 5 \times 1$ k-point mesh with lattice parameters $\mathbf{a}_1 = (a_{Cu}/\sqrt{2})(3,4,0) = (0.764, 1.018, 0.00)$ nm $(|\mathbf{a}_1| = 1.27$ nm$)$ and $\mathbf{a}_2 = (a_{Cu}/\sqrt{2})(-2,6,0) = (-0.509, 1.528, 0.00)$ nm $(|\mathbf{a}_2| = 1.61$ nm$)$. In the last case, the vacuum layer region between consecutive slabs is 1.979 nm, thick enough to ensure negligible interactions between periodic images normal to the surface when we include the layer. The calculations are spin-restricted.

The top and lateral views of the optimized geometrical configuration of a monolayer of EP-PTCDI arranged on Cu(100) obtained with DFT are shown in Figure 3. It is
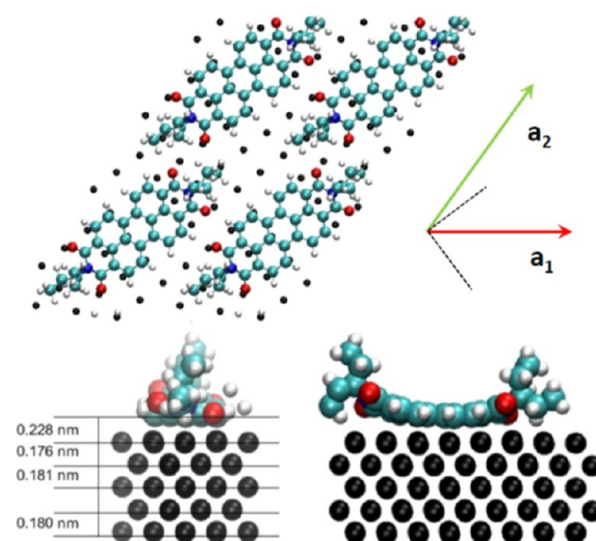
Figure 3. Calculated top and side views of the optimized geometrical configuration of EP-PTCDI/Cu(100).

observed that the perylene core approaches the surface up to about 0.2 nm remaining quasi parallel (slightly bended) to the Cu surface. This pushes up the EP-end groups out of the core plane, orienting them almost perpendicular to the surface plane.

To get more details on the arrangement of the molecules within a single domain, molecular-resolved STM images have been acquired. In Figure 4, we show an STM image with good
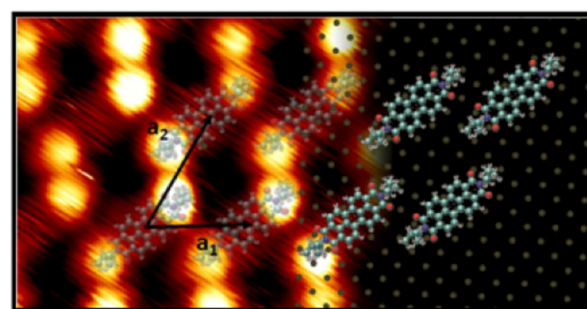
Figure 4. Molecular-resolved STM image (5×4 nm^2) and schematic representation of EP-PTCDI molecules deposited on Cu(100). The STM image was acquired at $V_S = -1.0$ V and $I_T = 60$ pA.

resolution of the EP-PTCDI molecule, allowing us to identify individual molecules as two bright spots joined at the opposite ends of an oval-like structure. For comparison, a schematic representation of the scaled calculated molecule has been superimposed to the STM image. By this comparison one can conclude that the spots correspond to the EP- end groups pushed out of plane. The oval structure width is about 0.75 nm; the total molecular length is approximately 2.20 nm; and the center-to-center distance between the two bright spots of a single molecule is about 1.30 nm, in very good agreement with the calculated EP-PTCDI molecule shown in Figures 3 and 4.
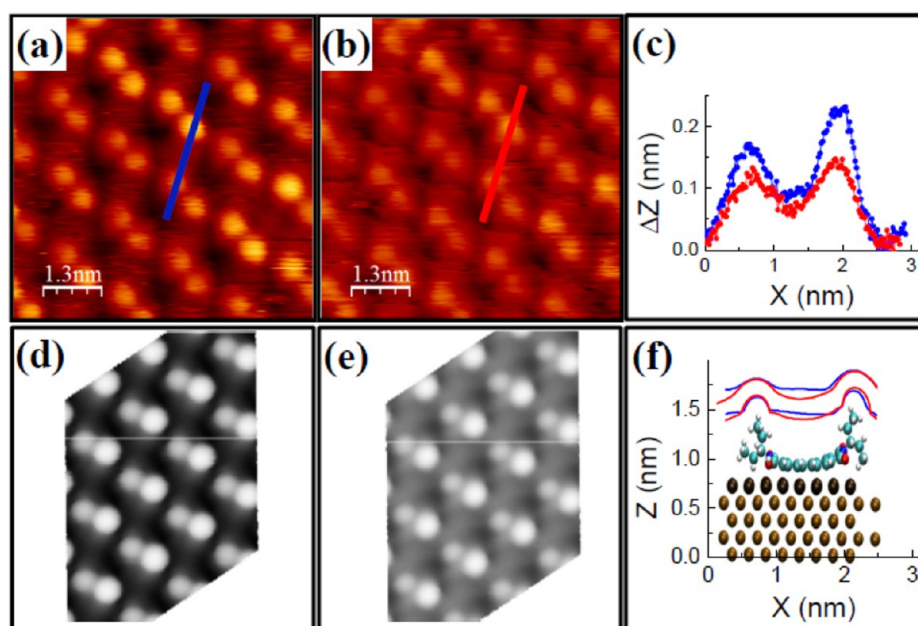
Figure 5. STM dual-scan-mode images of EP-PTCDI deposited on Cu(100) obtained simultaneously in the forward (a) $V_S = -1.0$ V and backward (b) $V_S = +1.0$ V directions. The images were acquired at $I_T = 60$ pA. (c) Scan profiles acquired along the lines drawn in panels (a) and (b). Partial charge isodensity images (isodensity value of 5×10^{-5} states/(unit cell volume)) obtained after integration of the electron states up to -1 eV (d) and to $+1$ eV (e) with respect to the Fermi level. (f) Side view of the optimized geometrical configuration of 1 ML of EP-PTCDI on Cu(100), together with the height profiles obtained along a single molecule on images of panels (d) and (e). The upper (lower) curves correspond to an isodensity value of 5×10^{-5} (5×10^{-3}) states/(unit cell volume).

To study the effects of the electronic structure of the system in the STM images, zoomed areas in a dual-scan mode have been acquired. In this acquisition mode, two STM images can be recorded at the same time by applying different bias voltages in the forward and backward fast scan directions. This method allows us to obtain information not only on the arrangement of the molecules but also on the differences in the iso-current spatial distribution of empty and filled electron states around them. In Figure 5, we show two STM images acquired simultaneously in the dual-scan mode at bias voltages of (a) $V_S = -1.0$ V (filled states) and (b) $V_S = +1.0$ V (empty states) with a tunnelling current of 60 pA, for the molecular arrangement of islands labeled 1. The STM image acquired at -1.0 V (Figure 5a) shows a good resolution of the EP-PTCDI molecule, allowing us to clearly identify individual molecules. On the other hand, the STM image acquired at $+1.0$ V (Figure 5b) shows a less defined molecular structure with fuzzy bright spots and the oval structure not clearly visible. Figure 5c shows the height profiles of single molecules acquired along the lines drawn in the images of panels (a) and (b). For molecules recorded at -1.0 V, the two bright spots show different heights with a difference of about 0.07 nm, and for those recorded at $+1.0$ V this difference is smaller, of about 0.02 nm.

By means of DFT calculations, the partial charge density within the electronic band energy range between the Cu(100) Fermi energy and ± 1 eV was evaluated. In the Tersoff–Hamann approach[29] this partial charge density is proportional to the tunneling current at the position of the STM tip when the bias voltages are ± 1 V, respectively. In panels (d) and (e) of Figure 5, we show the simulated STM images corresponding to $+1$ V and -1 V with an isodensity value of 5×10^{-5} states/(unit cell volume). In panel (f) we plotted the height profiles taken from the simulated STM images along a single molecule (similar to what we did with the experimental results), for

isodensity values of 5×10^{-3} and 5×10^{-5} states/(unit cell volume). A side view of the molecular arrangement on the surface is also shown in this panel. The trends observed in the experimental profiles are better reproduced by the profiles calculated for 5×10^{-5} states/(unit cell volume), so the simulated STM images shown in panels (d) and (e) were presented for this isodensity value.

The comparison of the experimental and calculated STM images and height profiles clearly shows that the brighter spots correspond to the rotated EP-end groups as it was suggested before. The center-to-center distance measured between the end groups (bright spots) in a single molecule (1.30 nm) agrees very well with that obtained in the simulation (1.39 nm). On the other hand, even when the absolute values of the simulation are higher than the experimental one, the general trends observed in the experiment are well reproduced by the calculations: the heights of the EP-end groups within a single molecule are different, and the heights between the EP-end groups and the PTCDI core are higher in images taken at -1 V than in those taken at $+1$ V. In addition, the simulated STM images agree pretty well with those measured in the dual-scan mode: the -1 V image shows a single molecule formed by two bright spots joined through an oval-like structure, and the assembly between consecutive molecules presents a double spot formed by the end groups of two distinct molecules that have different heights. As in the experiments, in the $+1$ V simulated STM images, these differences are less pronounced.

The XPS spectra measured for 1, 3, and 20 equivalent monolayers of EP-PTCDI deposited on Cu(100) are shown in Figure 6. By integration of the XPS peaks we verified that the ratios of O, N, and C areas (corrected by sensitivity factors) agree with the expected stoichiometry of the EP-PTCDI molecule ($C_{34}H_{30}N_2O_4$). The C 1s spectrum shows a main structure centered at 285.8 eV and smaller structures at 287.8
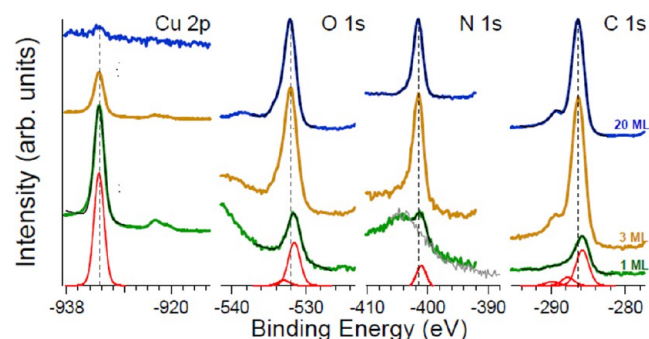
Figure 6. XPS spectra measured for 1, 3, and 20 equivalent layers of EP-PTCDI over a Cu(100) surface. The spectra at the bottom of the panels correspond to the fitting of 1 ML experimental data. For comparison, the 20 ML spectra were divided by a factor of 2.15.

Figure 7. (a) Work function changes measured with the onset shift of the low energy secondary electron spectra. (b) Calculated electrostatic potentials with respect to the Fermi energy as a function of the distance perpendicular to the surface.

and 289.9 eV, at 1 ML coverage. The principal structure is associated to the C atoms in the aromatic environment and in the EP tails, while the smaller high binding energy features are ascribed to the carbon atoms of the imide groups.[18] The O 1s spectrum presents a main structure at 531.6 eV and a small shoulder at around 533 eV, which is associated to the shake up satellite of the main feature.[14,34] Finally, the N 1s spectrum presents a peak at 401.1 eV.

The comparison of the energy position of the peaks measured for one monolayer with respect to those obtained for a multilayer shows a clear shift of about 0.5−0.6 eV for N 1s, O 1s, and C 1s. The shift to lower binding energies when one monolayer is adsorbed is attributed to a higher screening of the core hole final state produced by a charge transfer from the substrate metal electrons to the EP-PTCDI molecule.[18] The similar shifts observed for the three types of atoms described before indicate that all of them receive electronic charge. In agreement with the experimental results, DFT calculations showed charge transfer from the surface to N, O, and C atoms with a total charge transfer to the molecule of about 1.4 electrons/molecule.

The charge transfer from the surface to the molecule results in an excess of negative charges outside the Cu clean surface. In a first interpretation, this will produce an increase of the original surface dipole due to electron "spill out" in the Cu(100) surface. As a consequence, one would expect a work function increase.[35,36] However, the work function changes measured with the variation of the onset of the low energy secondary electron emission shows a decrease of about 0.70 eV when 1 ML of EP-PTCDI molecules is deposited on the surface (Figure 7a). Taking into account that the sample work function of the Cu(100) surface is 4.59 eV,[37] the value with the molecular layer results as 3.9 eV. The change of the work function after adsorption results from the modification of the Fermi energy and the dipolar layer, the last one described by the asymptotic electrostatic potential. The electrostatic potential with respect to the Fermi energy along the surface for the clean Cu and the monolayer of EP-PTCDI adsorbed on the same surface was calculated with DFT. The results are shown in Figure 7b, where we found a very good agreement between the calculated (0.67 eV) and the measured work function change (0.7 eV).

To get some insight into the reason for this change in the work function, the variations of the electrostatic potential and the charge density due to the interaction are discussed. The electrostatic potential of 1 ML of EP-PTCDI adsorbed on
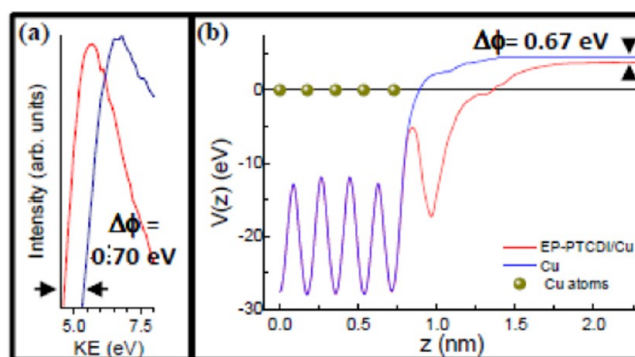
Cu(100) can be written as: $V^{mol/Cu}(z) = V^{mol}(z) + V^{Cu}(z) + \Delta V(z)$, where $V^{mol/Cu}(z)$ is the electrostatic potential after the adsorption and $V^{mol}(z)$ and $V^{Cu}(z)$ are the electrostatic potentials for the molecular arrangement without the substrate and the clean Cu surface, respectively. $\Delta V(z)$ accounts for the contribution due to the interaction after the adsorption. On the other hand, we can consider the effect of the adsorption on the charge density (ρ) by defining the change of the charge density as: $\Delta\rho(z) = \rho^{mol/Cu}(z) - (\rho^{mol}(z) + \rho^{Cu}(z))$. Note that $V(z)$ and $\rho(z)$ were obtained as a function of the distance to the surface by integration within planes parallel to the surface and were calculated on the same unit cell.

Since the experimental work function change ($\Delta\Phi$) has been measured with respect to the clean Cu surface, $\Delta\Phi$ has to be calculated as

$$\Delta\Phi = V^{mol/Cu}(\infty) - V^{cu}(\infty)$$
$$= V^{mol}(\infty) + \Delta V(\infty)$$
$$\rightarrow \Delta V(\infty) \tag{1}$$

and as the molecule does not have an intrinsic dipole, $V^{mol}(z \rightarrow \infty) \rightarrow 0$, the net change of the work function results from $\Delta V(\infty)$.

In Figure 8a we show the electrostatic potential $\Delta V(z)$ as a function of the distance to the surface. It presents a strong variation along the selvedge region (within the Cu−molecule interface) and asymptotically decreases to the value of the measured work function change.

The electrostatic potentials of the copper sample as a function of the distance to the surface, before ($V^{Cu}(z)$) and after one EP-PTCDI monolayer adsorption ($\Delta V^{Cu}(z) = V^{mol/Cu}(z) - V^{mol}(z)$), are presented in Figure 8b. Comparing both curves, we observe that the perturbation generated by the molecular adsorption produces the following effects on the clean metal potential: a reduction around the topmost Cu layer, a strong increase in the interface followed with a fast attenuation at the molecular core layer, and finally, a reduction of the asymptotic potential value. Since all these properties can be related with the changes in the charge density, we have also plotted $\Delta\rho(z)$ in Figure 8d. There, we observe that the adsorption of the molecular layer causes a rearrangement of the electron distribution: there are less electrons around the topmost Cu atoms, more electrons within the interface, and oscillations of the charge density at the molecular layer. These results indicate that, even when there is an increment of the Cu
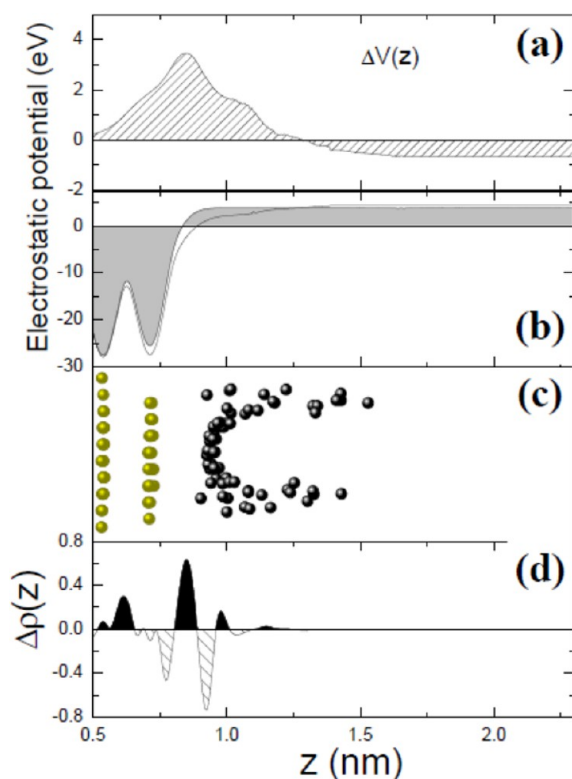
Figure 8. Electrostatic potential and charge density as function of the distance to the surface: (a) Net change of the electrostatic potential $\Delta V(z)$. (b) Copper potential before (- -) and after (gray shades area) EP-PTCDI adsorption. (c) Geometrical configuration of EP-PTCDI on Cu(100). (d) Net charge density change $\Delta\rho^{mol}(z)$: black and shaded areas represent excess and defect of electrons, respectively.

surface dipole, the presence of the molecular layer "screens" the corresponding dipole potential, reducing its asymptotic value.

4. CONCLUSIONS

In this work, we have studied the adsorption kinetics and ordering from the very initial stages of growth of EP-PTCDI molecules adsorbed on Cu(100). We have shown that the molecular adsorption starts on the substrate's terraces, without a preferential nucleation at step-edges, subsequently forming islands that grow laterally to cover the substrate with one full monolayer. The molecular structure within the islands is commensurate with the substrate and can be represented by the matrix $\begin{pmatrix} 3 & 4 \\ -2 & 6 \end{pmatrix}$. The orientation of the islands with respect to the Cu(100) substrate corresponds to its four rotational equivalents.

Further, DFT calculations show the configuration of the molecule and confirm the stacking geometry of the monolayer observed by LEED and STM, giving in addition insights into the particular features (changes in the shape of the bright spots) observed in the STM images taken at different experimental conditions.

Finally, the results of electron spectroscopies and the DFT calculations show that there is about 1.4 electron/molecule charge transfer from the surface to the molecule, with a decrease of the work function of about 0.7 eV (from 4.59 to 3.9 eV) after the adsorption of one monolayer of EP-PTCDI on Cu(100).

The present results can be helpful for understanding the ordering and the growth mechanism of organic molecules on metal surfaces as well as for understanding the role of the chemical potential of the bare metal, of the metal surface dipole, and of the ionization potential and electron affinity of the organic layer to tune the charge injection barrier in optoelectronic devices.[38]

The results of the study of the thermal stability of EP-PTCDI thin films deposited on Cu(100) and of the arrangement of the remaining new single layer of dissociated molecules will be presented in a forthcoming paper.

■ AUTHOR INFORMATION

Corresponding Author

*Phone: +54 294 4445234. Fax: +54 294 4445299. E-mail: esanchez@cab.cnea.gov.ar.

Notes

The authors declare no competing financial interest.

■ REFERENCES

(1) Jones, B. A.; Ahrens, M. J.; Yoon, M.-H.; Facchetti, A.; Marks, T. J.; Wasielewski, M. R. High-Mobility Air-Stable n-Type Semi-conductors with Processing Versatility: Dicyanoperylene-3,4:9,10-bis(DiCarboxImides). *Angew. Chem., Int. Ed.* **2004**, *43*, 6363−6366.

(2) Jonkheijm, P.; Stutzmann, N.; Chen, Z.; de Leeuw, D. M.; Meijer, E. W.; Schenning, A. P. H. J.; Würthner, F. Control of Ambipolar Thin Film Architectures by Co-Self-Assembling Oligo(p-phenylenevinylene)s and Perylene Bisimides. *J. Am. Chem. Soc.* **2006**, *128*, 9535−9540.

(3) Malenfant, P. R. L.; Dimitrakopoulos, C. D.; Gelorme, J. D.; Kosbar, L. L.; Graham, T. O.; Curioni, A.; Andreoni, W. N-Type Organic Thin-Film Transistor with High Field-Effect Mobility Based on a N,N′-Dialkyl-3,4,9,10-Perylene Tetracarboxylic Diimide Deriva-tive. *Appl. Phys. Lett.* **2002**, *80* (1−3), 2157.

(4) Gregg, B. A.; Cormier, R. A. Doping Molecular Semiconductors: n-Type Doping of a Liquid Crystal Perylene Diimide. *J. Am. Chem. Soc.* **2001**, *123*, 7959−7960.

(5) Breeze, A. J.; Salomon, A.; Ginley, D. S.; Gregg, B. A.; Tillmann, H.; Hörhold, H. H. Polymer−Perylene Diimide Heterojunction Solar Cells. *Appl. Phys. Lett.* **2002**, *81* (1−3), 3085.

(6) Alibert-Fouet, S.; Dardel, S.; Bock, H.; Oukachmih, M.; Archambeau, S.; Seguy, I.; Jolinat, P.; Destruel, P. Electroluminescent Diodes from Complementary Discotic Benzoperylenes. *Chem. Phys. Chem.* **2003**, *4*, 983−985.

(7) Schouwink, P.; Schäfer, A. H.; Seidel, C.; Fuchs, H. The Influence of Molecular Aggregation on the Device Properties of Organic Light Emitting Diodes. *Thin Solid Films* **2000**, *372*, 163−168.

(8) Zukawa, T.; Naka, S.; Okada, H.; Onnagawa, H. Organic Heterojunction Phototransistor. *J. Appl. Phys.* **2002**, *91* (1−4), 1171.

(9) Li, X.; Sinks, L. E.; Rybtchinski, B.; Wasielewski, M. R. Ultrafast Aggregate-to-Aggregate Energy Transfer within Self-assembled Light-Harvesting Columns of Zinc Phthalocyanine Tetrakis-(Perylenediimide). *J. Am. Chem. Soc.* **2004**, *126*, 10810−10811.

(10) Ruiz Delgado, M. C.; Kim, E.-G.; da Silva Filho, D. A.; Bredas, J.-L. Tuning the Charge-Transport Parameters of Perylene Diimide Single Crystals via End and/or Core Functionalization: A Density Functional Theory Investigation. *J. Am. Chem. Soc.* **2010**, *132*, 3375−3387.

11684

dx.doi.org/10.1021/jp402494j | *J. Phys. Chem. C* 2013, 117, 11679−11685

(11) Schmidtke, J. P.; Friend, R. H.; Kastler, M.; Müllen, K. Control of Morphology in Efficient Photovoltaic Diodes from Discotic Liquid Crystal. *J. Chem. Phys.* **2006**, *124* (1−6), 174704.

(12) Zhang, X.; Sun, B. Organic Crystal Fibers Aligned into Oriented Bundles with Polarized Emission. *J. Phys. Chem. B* **2007**, *111*, 10881−10885.

(13) Glöckler, K.; Seidel, C.; Soukopp, A.; Sokolowski, M.; Umbach, E.; Böhringer, M.; Berndt, R.; Schneider, W.-D. Highly Ordered Structures and Submolecular Scanning Tunnelling Microscopy Contrast of PTCDA and DM-PBDCI Monolayers on Ag(111) and Ag(110). *Surf. Sci.* **1998**, *405*, 1−20.

(14) Zahn, D. R. T.; Gavrila, G. N.; Salvan, G. Electronic and Vibrational Spectroscopies Applied to Organic/Inorganic Interfaces. *Chem. Rev.* **2007**, *107*, 1161−1232.

(15) Horcas, I.; Fernández, R.; Gómez-Rodríguez, J. M.; Colchero, J.; Gómez-Herrero, J.; Baró, A. M. WSXM: A Software for Scanning Probe Microscopy and a Tool for Nanotechnology. *Rev. Sci. Instrum.* **2007**, *78* (1−8), 013705.

(16) Im Langenbroich 20-D-52428 Juelich, Germany. http://www.mateck.de/.

(17) ChemiePark, Areal A Sensientstrasse 3 D-06766 Wolfen, Germany.

(18) Serkovic Loli, L. N.; Hamoudi, H.; Gayone, J. E.; Martiarena, M. L.; Sánchez, E. A.; Grizzi, O.; Pasquali, L.; Nannarone, S.; Doyle, B. P.; Dablemont, C.; Esaulov, V. A. Growth of *N*,*N*′-Bis(1-ethylpropyl)-perylene-3,4,9,10-tetracarboxdiimide Films on Ag(111). *J. Phys. Chem. C* **2009**, *113*, 17866−17875.

(19) Serkovic Loli, L. N.; Sánchez, E. A.; Gayone, J. E.; Grizzi, O.; Esaulov, V. A. Assembly and Thermal Stability of Thin EP-PTCDI Films on Ag(111). *Phys. Chem. Chem. Phys.* **2009**, *11*, 3849−3853.

(20) Kresse, G.; Hafner, J. Ab Initio Molecular Dynamics for Liquid Metals. *Phys. Rev. B* **1993**, *47*, 558−561.

(21) Kresse, G.; Hafner, J. Ab Initio Molecular-Dynamics Simulation of the Liquid-Metal−Amorphous-Semiconductor Transition in Germanium. *Phys. Rev. B* **1994**, *49*, 14251−14269.

(22) Blöchl, P. E. Projector Augmented-Wave Method. *Phys. Rev. B* **1994**, *50*, 17953−17979.

(23) Perdew, J. P.; Wang, Y. Accurate and Simple Analytic Representation of the Electron-Gas Correlation Energy. *Phys. Rev. B* **1992**, *45*, 13244−13249.

(24) Dion, M.; Rydberg, H.; Schröder, E.; Langreth, D. C.; Lundqvist, B. I. Van der Waals Density Functional for General Geometries. *Phys. Rev. Lett.* **2004**, *92* (1−4), 246401.

(25) Román-Pérez, G.; Soler, J. M. Efficient Implementation of a van der Waals Density Functional: Application to Double-Wall Carbon Nanotubes. *Phys. Rev. Lett.* **2009**, *103* (1−4), 096102.

(26) Monkhorst, H.; Pack, D. Special Points for Brillouin-Zone Integrations. *Phys. Rev. B* **1976**, *13*, 5188−5192.

(27) Methfessel, M.; Paxton, A. T. High-Precision Sampling for Brillouin-Zone Integration in Metals. *Phys. Rev. B* **1989**, *40*, 3616−3621.

(28) Henkelman, G.; Arnaldsson, A.; Jónsson, H. A Fast and Robust Algorithm for Bader Decomposition of Charge Density. *Comput. Mater. Sci.* **2006**, *36*, 354−360. Sanville, E.; Kenny, S. D.; Smith, R.; Henkelman, G. Improved Grid-Based Algorithm for Bader Charge Allocation. *J. Comput. Chem.* **2007**, *28*, 899−908.

(29) Tersoff, J.; Hamann, D. R. Theory of the Scanning Tunneling Microscope. *Phys. Rev. B* **1985**, *31*, 805−813.

(30) Lee, K.; Murray, E. D.; Kong, L.; Lundqvist, B. I.; Langreth, D. C. Higher-Accuracy van der Waals Density Functional. *Phys. Rev. B* **2010**, *82* (1−4), 081101.

(31) Hlawacek, G.; Puschnig, P.; Frank, P.; Winkler, A.; Ambrosch-Draxl, C.; Teichert, C. Characterization of Step-Edge Barriers in Organic Thin-Film Growth. *Science* **2008**, *321*, 108−111.

(32) Hermann, K.; van Hove, M. A. See: http://w3.rz-berlin.mpg.de/~hermann/LEEDpat/.

(33) Klimeš, J.; Bowler, D. R.; Michaelides, A. Van der Waals Density Functionals Applied to Solids. *Phys. Rev. B* **2011**, *83* (1−13), 195131.

(34) Zou, Y.; Kilian, L.; Schöll, A.; Schmidt, Th.; Fink, R.; Umbach, E. Chemical Bonding of PTCDA on Ag Surfaces and the Formation of Interface States. *Surf. Sci.* **2006**, *600*, 1240−1251.

(35) Ishii, H.; Sugiyama, K.; Ito, E.; Seki, K. Energy Level Alignment and Interfacial Electronic Structures at Organic/Metal and Organic/Organic Interfaces. *Adv. Mater.* **1999**, *11*, 605−625.

(36) Braun, S.; Salaneck, W. R.; Fahlman, M. Energy-Level Alignment at Organic/Metal and Organic/Organic Interfaces. *Adv. Mater.* **2009**, *21*, 1450−1472.

(37) Gartland, P. O.; Berge, S.; Slagsvold, B. J. Photoelectric Work Function of a Copper Single Crystal for the (100), (110), (111), and (112) Faces. *Phys. Rev. Lett.* **1972**, *28*, 738−739.

(38) Crispin, X.; Geskin, V. M.; Crispin, A.; Cornil, J.; Lazzaroni, R.; Salaneck, W. R.; Brédas, J.-L. Characterization of the Interface Dipole at Organic/Metal Interfaces. *J. Am. Chem. Soc.* **2002**, *124*, 8131−8141.